Environmental Science & Technology

pubs.acs.org/est

Article

A Quantitative Relationship between Settling and Wettability for Weathered Microplastics in Aquatic Systems

Yi Liang, Jingyi Gu, Ketong Chen, Hong Zhou, Jiamin Peng, Tingting Cai, Pei Na, Chenlu Guo, Weilin Huang, Chen Yang,* and Zhi Dang

Cite This: https://doi.org/10.1021/acs.est.4c11053

Read Online

ACCESS | Metrics & More | Article Recommendations | Supporting Information

ABSTRACT: Settling plays a crucial role in determining the residence time, distribution, transport, and ultimate fate of microplastics (MPs) in aquatic environments. The settling dynamics of particles are influenced by their macroscale shape, mesoscale roundness, and microscale surface properties, along with ambient fluid flow conditions. Variations in the wettability of submillimeter MPs affect molecular interactions at the particle−water interface, altering the microscopic flow field and subsequently modifying drag forces during settling. This study examines the impact of wettability on the settling behavior of aged acrylonitrile butadiene styrene MPs by measuring their settling velocities and contact angles. It was shown that increased wettability promotes the settlement of the MPs. A drag model incorporating the Eötvös number—a dimensionless ratio of buoyancy energy to contact angle-derived surface energy—is developed to quantify the relationship between interfacial chemistry and hydrodynamic resistance. Unlike the conventional models, our model considers wettability as a key factor controlling the settling of MP particles. The model was validated using independently measured data and four sets of published data for the MPs. Results demonstrate that the model significantly improves the accuracy of the settling predictions for weathering spherical MPs. Additionally, by integrating the shape factor, it effectively accounts for the settling behavior of irregularly shaped MPs using published data sets. This improvement enhances predictability for MP transport pathways, helping assess MP accumulation zones and potential ecological risks in marine and freshwater systems.

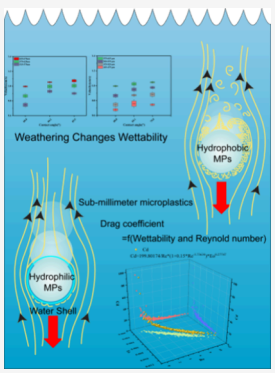

KEYWORDS: *microplastics, terminal velocity, drag coefficient, surface wettability, interfacial tensions*

1. INTRODUCTION

Microplastics (MPs) are widely found in ecosystems partly due to their resistance to degradation and high mobility. These particles can be transported over long distances to remote regions, including polar ecosystems (Arctic and Antarctica),[1−3] where they ultimately accumulate in both marine and terrestrial environments. Due to their small sizes, MPs are prone to ingestion by aquatic organisms, leading to gastrointestinal blockages and broader physiological disruptions.[4,5] The transport of MPs is influenced by the interaction between their specific physicochemical properties and the surrounding hydrodynamic conditions. While hydrodynamic forces control horizontal advection and dispersion, vertical transport is primarily determined by the particles' physicochemical characteristics. Understanding the environmental behavior and long-term fate of MPs remains both scientifically critical and mechanistically complex.

For negatively buoyant MPs (e.g., polyvinyl chloride, acrylonitrile butadiene styrene (ABS), polystyrene) and neutrally buoyant particles (e.g., polyethylene, polypropylene), settling kinematics govern vertical stratification and inform transport-diffusion models. The terminal settling velocity influences MP residence time, depth-specific concentration gradients, and their trophic transfer within aquatic food webs.[6,7] Predicting this parameter accurately is key for source apportionment of plastic pollutants,[8] which is vital for remediation strategies and risk assessment.

Unlike mineral-based sediments, MPs undergo relatively faster weathering processes such as UV photodegradation, mechanical abrasion, and biofouling,[9−13] leading to morphological changes, density variations, and surface property modifications.[14−16] These alterations cause settling behaviors distinct from those of unweathered MP particles. While previous research identified particle morphology, size, and density as key factors in settling velocities,[17,18] existing drag models fail to account for the effects of MP weathering processes.[19−21] Recent studies of MP settling mainly focus on shape and density, neglecting surface chemistry effects.

It is intuitive that weathering can impact MP settling behavior,[19,22] but critical gaps remain in understanding such effects by surface property changes.[23−25] Drag forces result

Received: October 15, 2024
Revised: May 12, 2025
Accepted: May 13, 2025

from viscous interactions at the particle-fluid interface, where wettability and surface roughness alter boundary layer dynamics.[26−28] These changes affect local flow, modulating viscous resistance and settling velocities—critical for vertical transport.[16,29] Recent evidence shows that hydrophilic/hydrophobic transitions significantly influence settling dynamics,[30,31] underscoring the need for surface-aware drag models. ABS-based MPs, widely present in aquatic environments due to their high mechanical stability,[32−34] were selected as the model MPs in this study. Common environmental weathering processes—such as UV exposure, mineral deposition, and chlorination—were simulated, each of which resulted in irreversible surface modifications and altered wettability.[35] However, existing drag models do not account for hydrophilic/hydrophobic changes in MPs, potentially leading to biased predictions of their distribution and increased uncertainty in assessing their long-term fate in aquatic systems. To date, the influence of wettability on the MP settling behavior remains poorly quantified.

To address this knowledge gap, we conducted a study to examine how weathering-induced changes in surface wettability affect the settling dynamics of MP particles in aquatic environments. The settling velocities and contact angles were measured under hydrostatic conditions for the weathered spherical ABS-MPs. A drag model was developed that incorporates the Eötvös number—a dimensionless ratio of buoyancy energy to contact angle-derived surface energy—for establishing a relationship between wettability and hydrodynamic resistance. Independently measured data and four sets of published data for MPs were used for validating the model. Results demonstrate that our model significantly improves the accuracy of the settling predictions for spherical MPs. Additionally, by integrating a shape factor and using published data, the model can effectively predict the settling behavior for irregularly shaped MPs. This study not only offers a quantitative tool for assessing wettability effects on MP settling but also enhances our understanding of particle transport processes in aquatic systems.

2. MATERIALS AND METHODS

2.1. Materials, Microplastic Weathering, Characterization, and Contact Angle Measurements. The spherical MPs used in this study were obtained commercially from suppliers on online platforms (ABS, −COOH, and $-NH_2$). ABS was purchased from Zhangmutou Suzhan Plastic Operations (Dongguan City, Guangdong Province). Functionalized PS was obtained from Zhichuan Intelligent Technology (Suzhou) Co., Ltd. Certified polystyrene microspheres were purchased from Thermo Fisher Scientific Inc. Goethite and octadecyl trichlorosilane (OTS) were purchased from Aladdin Ltd. in Shanghai. Sodium hypochlorite (7.5% available chlorine, AR) was purchased from Shanghai Titan Technology Co., Ltd.

Four representative surface modifications for MPs were implemented to simulate environmentally relevant MP aging pathways: (i) UV photooxidation (UV) mimicking solar degradation; (ii) sodium hypochlorite treatment (GL) replicating wastewater disinfection processes; (iii) goethite heteroaggregation (GT) modeling mineral−MP interactions; (iv) the OTS emulating engineered hydrophobic surfaces.

Before being weathered, the fresh ABS MPs were thoroughly rinsed with RO-treated high purity water and air-dried. Samples were stored in the dark at room temperature and labeled as untreated MPs (origin, −COOH, $-NH_2$). To identify the types of commercial plastics, an attenuated total reflection Fourier transform infrared (ATR-FTIR) was applied to determine the chemical composition of the cleaned MP (Figure S2). All MPs including the fresh and weathered particles were assessed in the laboratory for size and size distribution, chemical composition, and mechanical integrity. The densities of the MPs were estimated using the titration method outlined in ISO 1183-1 (Section S1, page S3).

2.1.1. UV Aging (UV). Original ABS-MPs were placed in glass Petri dishes and exposed to UV light (UVC-254 nm, 35 mW/cm^2) for 3 days (UV-3 Day), 7 days (UV-7 Day), and 10 days (UV-10 Day), at a constant temperature of 25 ± 2 °C in a light chamber.

2.1.2. Chlorination (GL). A 1.0 g portion of the original ABS was immersed in 100 mL of sodium hypochlorite solution at 60.0 °C for 1.0 h. The solid was obtained by filtering through filter paper, washed several times with RO water, and air-dried. The effective chlorine concentrations used for the experiments were 2.0 g/L (2GL) and 4.0 g/L (4GL).[36]

2.1.3. Goethite Deposition (GT). A 100 mg portion of the original ABS was weighed, and the goethite (2, 5, 10, 100 mg) and 50 mL of deionized water were added to create mass ratios of goethite to MPs 1:50 (2GT), 1:20 (5GT), 1:10 (10GT), and 1:1 (100GT), respectively. After shaking at 25 °C for 24 h at 150 rpm, the sample was obtained by filtering with filter paper and dried naturally.

2.1.4. Surface Modification with Octadecyl Trichlorosilane (OTS). OTS is used to simulate the daily use of highly hydrophobic polymers, such as fiberglass cloth.[37] Two milliliters of OTS (4.6 mmol) were mixed with 40 μL (2.2 mmol) of water, vortexed, and sonicated immediately. After 2 h at room temperature, the mixture was diluted with hexane (5% v/v OTS/hexane) and sprayed onto the surface of the original ABS using a spray bottle.[38]

Surface topography was characterized via 3D optical profilometry (Sensofar S neox 090) to obtain Sa roughness parameters, while wettability was quantified through static contact angle measurements by using a sessile drop method (DataPhysics OCAH200). Particulate contact angles were determined by the powder compression technique (detailed protocols in Section S1, page S3).

2.2. Settling Experiments. The sinking experiment was conducted in a temperature-controlled room to avoid fluctuations in the viscosity of the medium during measurements. The terminal settling velocities were measured at 25 ± 0.5 °C in a poly(methyl methacrylate) sedimentation column (0.2 × 0.2 × 0.6 m, $L \times W \times H$; Figure S1). Due to the large internal diameter of the column, wall effects can be neglected. Before testing, MP particles were submerged in RO water for 24 h in sealed scintillation vials to mitigate electrostatic surface charge interference. The particles were released at the center of the column from a rubber-tipped dropper approximately 5 cm below the surface of the water. To avoid turbulent disturbances, the particles sink from the dropper in free fall. Video acquisition was achieved using an industrial CMOS camera (LT-USB1080P) with a 30 fps capability coupled to a lens (LT-CS055016−3MP). An LED backlight was positioned behind the water column to create a shadow of the settling particles.[21] From the recorded videos, still image sequences depicting the settling kinematics were extracted at intervals of 1/30 s using MATLAB. The settling distance and diameter of each particle were measured from these sequential images at

https://doi.org/10.1021/acs.est.4c11053
Environ. Sci. Technol. XXXX, XXX, XXX−XXX

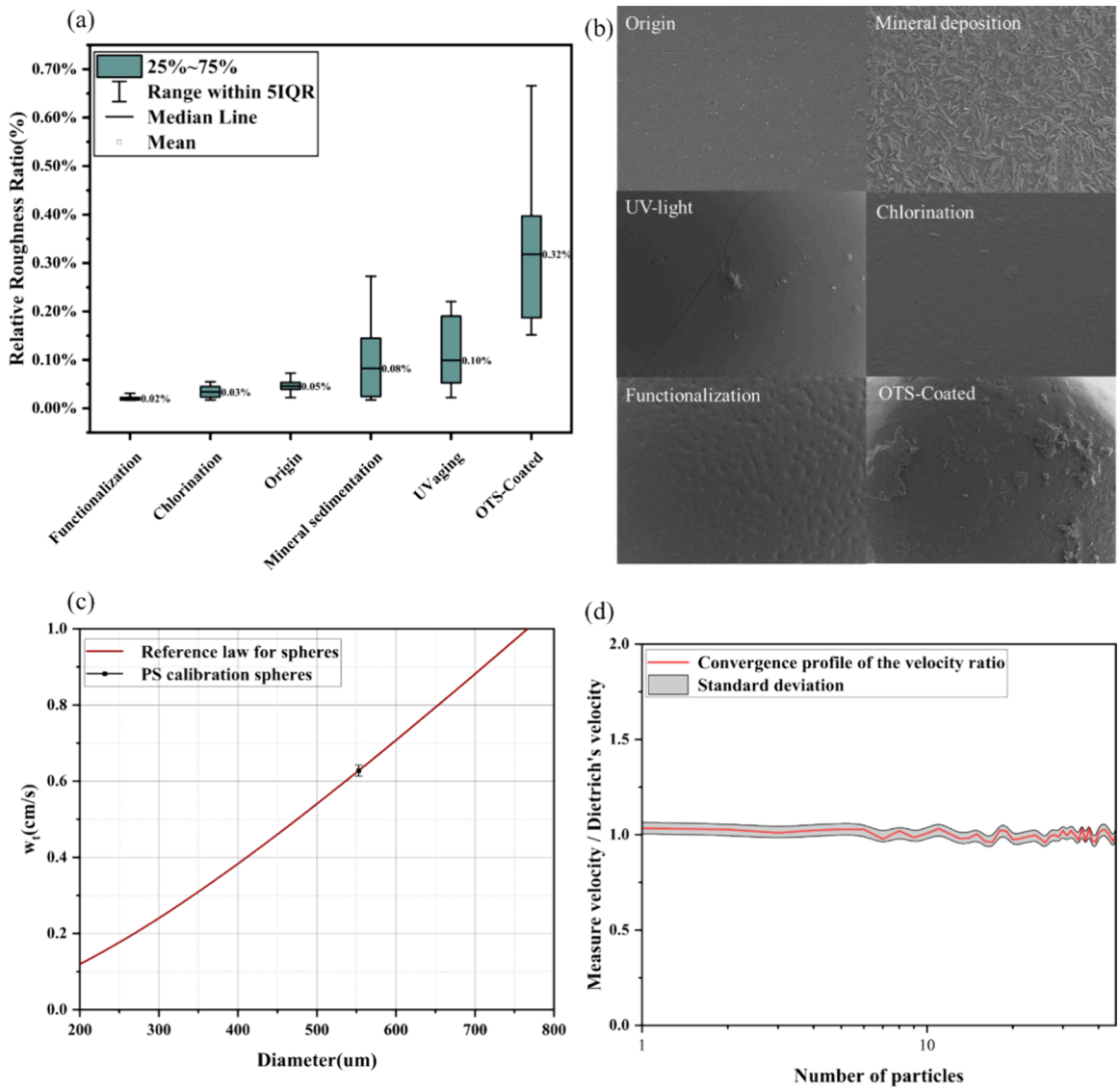

Figure 1. (a) Relative roughness ratio of weathering MPs. (b) Surface morphology of weathering MPs. (c) Measured settling velocities of the certified PS calibration spheres (1050 kg·m^{-3}, 553 ± 11 μm. Duke Standards, NIST Traceable Mean Diameter, Thermo Fisher Scientific, Germany). Illustrating the fit to the reference law for spheres proposed by Dietrich (1982). (d) Assessment of the column setup, particle tracking, image acquisition, and data postprocessing. PS calibration spheres were used for the test, and the measured settling velocity was then compared with the theoretical settling velocity calculated by Dietrich's law.

known time intervals (i.e., 1/30 s) using the image measurement software ImageJ (https://imagej.net/ij/). The settling velocity of each particle was then calculated.

Methodological validation involved certified polystyrene microspheres (Φ = 553 ± 11 μm, ρ = 1.050 g/cm^3; Duke Standards 4355A, Thermo Fisher Scientific). Repetitive measurements of 50 times demonstrated <3% deviation from Dietrich's empirical model,[39] consistent with prior MP validation studies[40,41] (Figure 1).

2.3. Improved Surface Drag Model. The Reynolds number can be computed from the measured terminal settling velocity, the diameter of the particles, and the kinetic viscosity of the fluid:

$$\mathrm{Re} = \frac{d\rho_1 w_{t,mea}}{\mu_1} \tag{1}$$

The drag coefficient for a given particle can be calculated independently using the following equation:

$$C_{d,mea} = \frac{4d(\rho_s - \rho_1)g}{3\rho_1 w_{t,mea}^2} \tag{2}$$

where d, g, and $w_{t,mea}$ are the particle diameter, gravity constant, and particle settling velocity, respectively, and ρ_s and ρ_1 are, respectively, density of particle and water.

The dimensionless Eötvös number (Eo′, alternatively termed the Bond number) is defined as the ratio of buoyancy to surface tension forces:

$$\mathrm{Eo}' = \frac{gd^2(\rho_s - \rho_1)}{\gamma_{sl}} \tag{3}$$

Particles with high Eo′ values (Eo′ ≫ 1) settle in buoyancy-dominated regimes, where surface tension effects are negligible. In contrast, particles with low Eo′ values (Eo′ ≪ 1) remain stably suspended due to the dominance of surface tension

https://doi.org/10.1021/acs.est.4c11053
Environ. Sci. Technol. XXXX, XXX, XXX−XXX

forces.[42,43] Particles with intermediate Eo′ values experience a balance between these interfacial forces.

The surface free energy (γ_{sl}) was calculated from the model proposed by Zhu et al.[44] and Tang et al.[45] in the following equation:

$$\gamma_{sl} = \frac{\gamma_{lg}}{2}(\sqrt{1 + \sin^2\theta} - \cos\theta) \quad (4)$$

where γ_{lg} is 0.072 N/m representing water's surface tension and θ is the contact angle (in radians).

2.4. Data Established and Collection. The development of a surface-aware drag model (eq 7) for weathered MPs required the construction of a multiscale experimental database. The entire experimental data set obtained in this study consisted of 674 discrete settling experiments with concomitant contact angle measurements (full data set in the Supporting Information). For cross validation of the model, we used 50% of the entire data set (n = 341) (termed as data set 1) to develop the drag model. We used the remainders (n = 333) (data set 2) for internal validation. We also evaluated four independent data sets (data set 3, 4, 5, and 6) from four different studies (i.e., Goral et al.,[46] Dittmar et al.,[20] Lin et al.,[41] and Yu et al.,[47] respectively) and utilized them for external validation, with additional contact angle data curated from literature sources to calculate Eo′ (Table S1).[48−52]

To incorporate Eo′ into the existing model and enhance the generalizability of the model, data set 1 and data set 6 (n = 256 data) were used to derive an improved model (eq 8). The derivation process is illustrated in the Supporting Information (Figure S4).

2.5. Evaluation of the Existing Drag Models. Table 2 lists 13 models established based on the observations for unweathered MPs having different shapes. Many of these models could be used for predicting drag coefficients from particle density, shape, size, and Reynolds number, but fewer accounted for the effects of changes in particle surface properties during weathering of MPs in aquatic systems.

The models listed in Table 2 and the accuracy of the developed (eqs 7 and 8) models were evaluated for their predictability of drag coefficients using eqs 5 and 6. The experiment-based (data sets 1 and 2) and the model predicted values are used for calculating average relative error (AE) and the root-mean-square error (RMSE).

$$\mathrm{AE} = \frac{\sum_{i=1}^{N} \frac{|\mathrm{Cd}_{cal,i} - \mathrm{Cd}_{meas,i}|}{\mathrm{Cd}_{meas,i}}}{N} \times 100 \quad (5)$$

$$\mathrm{RMSE} = \sqrt{\frac{\sum_{i=1}^{N} \left(\frac{|\mathrm{Cd}_{cal,i} - \mathrm{Cd}_{meas,i}|}{\mathrm{Cd}_{meas,i}}\right)^2}{N}} \times 100 \quad (6)$$

Table 1. Basic Properties of MPs Used in Settling Experiments

treatment[a]	condition	density (g/cm^3)	contact angle (°)	particle size range (μm)	
origin	origin	1.080	88.2 ± 2.0	363.9	806.2
mineral deposition	2GT	1.084	89.3 ± 2.1	311.2	762.8
	5GT	1.080	85.9 ± 3.5	339.5	730.1
	10GT	1.086	86.2 ± 3.4	278.3	629.4
	100GT	1.129	82.8 ± 1.5	455.6	748.8
chlorination	2GL	1.079	85.1 ± 1.6	504.2	691.3
	4GL	1.077	79.8 ± 1.7	452.7	687.1
UV-aging	UV-3 Day	1.149	92.5 ± 1.8	351.4	588.0
	UV-7 Day	1.157	86.1 ± 2.6	310.8	627.3
	UV-10 Day	1.156	72.8 ± 3.2	364.2	652.9
surface treatment	−COOH	1.158	74.1 ± 2.5	477.9	847.1
	−NH_2	1.158	76.08 ± 2.1	557.2	889.4
	OTS	1.079	110.0 ± 2.8	401.5	656.6

[a]Mineral deposition: mass ratios of goethite to microplastics 1:50 (2GT), 1:20 (5GT), 1:10 (10GT), and 1:1 (100GT). Chlorination: concentrations used for the chlorination were 2.0 g/L (2GL) and 4.0 g/L (4GL). UV aging: 3 days (UV-3 Day), 7 days (UV-7 Day), and 10 days (UV-10 Day). OTS-coated (OTS) and functional grouping (−COOH, −NH_2).

3. RESULT AND DISCUSSION

3.1. Effect of Physical Properties on MP Settling. The settling velocity of MPs after weathering shows varying degrees of changes (Figure 2a−d). Specifically, the settling velocity increased after UV, chlorination, and mineral deposition, while the settling velocity decreased after hydrophobic coating. This variation can be attributed to the following factors.

3.1.1. Increasing in Density of the Polymer after Weathering. Table 1 shows that, after UV aging, the density of MPs increased by about 6%, from 1.08 ± 0.001 to 1.15 ± 0.005 g/cm^3 (Table 1), with an additional 4.5% increase after mineral deposition. UV irradiation disrupts the polymer chain structure, enhancing crystallinity and density, as noted by Alimi et al.[64] Consequently, the increased density contributes to a higher settling velocity, aligning with studies suggesting that UV aging enhances MP deposition in sediments.

3.1.2. Surface Property Modifications. Weathering may not only result in change in the density of the particles but also alter their surface properties. As MPs undergo aging, new polar functional groups may form on their surfaces, increasing their hydrophilicity. As a result, changes in the settling velocity of MPs cannot be attributed solely to increased density as surface property modifications may also play a significant role.[16] Lin et al. also found in their study that changes in the surface properties of MPs impact their settling behavior.[41]

3.1.3. Interfacial Hydrodynamics. Comparative analyses of drag coefficient (Cd) versus Reynolds number (Re) relationships (Figure 2e−h) reveal surface-dependent transport regimes. Hydrophobic OTS-coated MPs demonstrate elevated contact angles (θ = 110.0 ± 2.8°) and enhanced drag coefficients, reducing settling velocities compared to those of untreated controls (Figure 1d,h). This surface roughness amplifies viscous dissipation at the solid−liquid interface, creating turbulent boundary layers that impede settling.

Notably, mineral-deposited (excluding 100GT) and chlorinated MPs with comparable densities (1.08 ± 0.003 g/cm^3) exhibit higher settling velocities than pristine counterparts (Figure 2a,b, more details in the Supporting Information, Figure S5). Despite minimal density variation ($\Delta\rho$ < 0.01 g/cm^3), these treated particles experience reduced drag resistance (Figure 2e,f), indicating interfacial phenomena influent the hydrodynamic response.

To further characterize the effect of particle surface changes on the settling behavior of MPs, we compared the terminal velocities of MPs weathered using mineral deposition

https://doi.org/10.1021/acs.est.4c11053
Environ. Sci. Technol. XXXX, XXX, XXX−XXX

Table 2. Typical Drag Coefficient Models for Particles

researcher	drag coefficient formula	factor
Clift and Gauvin[53]	$Cd = \frac{24}{Re}(1 + 0.15Re^{0.687}) + \frac{0.42}{1 + \frac{42500}{Re^{1.16}}}$	Reynolds number
	$1 < Re < 10^3$	
Allen[54]	$Cd = \frac{18.5}{Re^{0.6}}$	Reynolds number
Zhiyao et al.[55]	$Cd = \left[\left(\frac{\sqrt{3}A}{2d_*^{3/2}}\right)^{2/n} + B^{1/n}\right]^n$	dimensionless diameter
	$A = 32.2\ B = 1.17\ n = 1.75$	
	where d_* is the dimensionless diameter.	
	$d_* = \left[\frac{(\rho_s - \rho_1)g}{\rho_1 \nu^2}\right]^{1/3} d_n$	
Cheng[56]	$Cd = \frac{432}{d_*^3}(1 + 0.022d_*^3)^{0.54} + 0.47[1 - \exp(-0.15d_*^{0.45})]$	dimensionless diameter
Alcerreca et al.[57]	$Cd = \frac{4}{3}\frac{d_*^3}{(\sqrt{22 + 1.13d_*^2} - 4.67)}$	dimensionless diameter
	$CSF = 0.11-0.98$, $Rep = 0.3-454.3$	
Song et al.[58]	$Cd = \frac{500}{d_*^3 \Phi^{0.98} S^{0.48}}(1 + 0.017d_*^3)^{0.6}$	sphericity, settling orientations
	Φ is the degree of sphericity.	
	$S = \frac{S_e}{S_p}$	
	S is the settling orientations. S_e is the surface area of the equivalent sphere, and S_p is the projected area of the particle in the settling direction.	
Khatmullina and Isachenko[59]	$Cd = \frac{\pi g D L}{2\nu(5.5283L + 12.691)}$	lengths
Waldschläger and Schüttrumpf[60]	$Cd(\text{pellets \& fragments}) = \frac{3}{CSF\sqrt{Re}}$	CSF shape factor
	$Cd(\text{fibers}) = \frac{4.7}{\sqrt{Re}} + \sqrt{CSF}$	
	$CSF = \frac{c}{\sqrt{ab}}$, where a, b, and c are the lengths of the longest, middle, and shortest sides of the particle, respectively.	
Wang et al.[29]	$Cd = \frac{24}{Re}\{e^{(-0.3+0.18\theta-0.02\theta^2)} + (2.3\theta + 1.32)e^{-\sqrt{Eo'}/[0.1\theta^{-0.99}]}\}^{-1}$	wettability; contact angle
	$Rep < 0.35$	
Wang et al.[61]	$w_s = 1.0434\left[\frac{(\rho_s - \rho_1)g}{\rho_1}\right]^{0.495} \frac{d_n^{0.777} CSF^{0.710}}{\nu^{0.124}}$	CSF shape factor; particle size
Yu et al.[47]	$Cd = \frac{\frac{432}{d_*^3}(1 + 0.022d_*^3)^{0.54} + 0.47[1 - \exp(-0.15d_*^{0.45})]}{(d_*^{-0.25} \Phi^{0.03d_*} CSF^{0.33d_*})^{0.25}}$	dimensionless diameter, CSF shape factor, sphericity
Zhang and Choi[62]	$Cd = \frac{58.58ASF^{0.1936}}{Re^{0.8273}}$	ASF shape factor
	$ASF = \frac{D_L}{D_S D_I}$, where D_L, D_I, and D_S are the longest, intermediate, and shortest lengths of a MP	
Meng and Li[63]	$Cd = 0.76 + \frac{97.23\left(\frac{k}{d_{MP}}\right)^{0.33}}{Re_p}$	roughness
	$\frac{k}{d_{MP}}$ is relative roughness ratio and k is the average peak-to-valley depth.	

(excluding 100 GT) and chlorination treatments, which have a constant density and different contact angles. Figure 3a,b indicates that contact angles are inversely related to particle settling velocity, suggesting MP particles having smaller contact angles and hence being more hydrophilic can settle as faster velocities in water.

The inverse relationship between contact angles and settling velocity could be explained via molecular interactions at the microscopic interface. In general, particle settling can be viewed as fluid flowing around the particles, where a boundary layer (a thin fluid layer adjacent to the surface) forms on the particle surface. During the slow settling process, the effects of viscous forces within this boundary layer cannot be neglected.[65] Surfaces transitioning from hydrophobic to hydrophilic nature can alter viscous forces and characteristics of the surrounding aqueous fluid as hydrophilic surfaces tend to be less resistant to water.

Moreover, smaller particles tend to exhibit more pronounced interfacial interactions. Typically, alterations in the wettability of particles modify the gravitational effects of the particles on water molecules. When the hydrophilicity of an MP surface increases, it lowers the free energy barrier for water absorption on its surface and alters the interaction of its surface with water molecules, thus tends to form a water shell on the plastic surface.[66] As a result, water molecules can slide more easily along the hydrophilic surface, reducing the thickness of the boundary layer and hence decreasing microturbulence of particle surface flow. The lowered ratio of inertial to viscous forces may keep the flow within the laminar regime, resulting in faster particle settling. Therefore, as the contact angle decreases, the drag on the particles decreases and the settling

https://doi.org/10.1021/acs.est.4c11053
Environ. Sci. Technol. XXXX, XXX, XXX−XXX

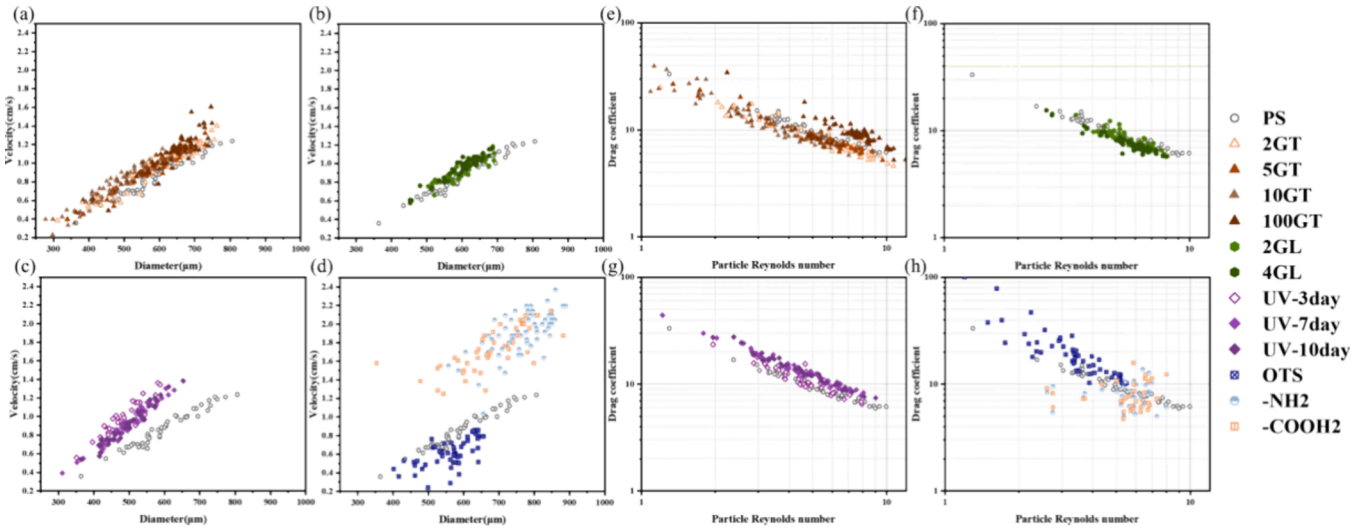

Figure 2. (a−d) Particle settling velocity as a function of particle diameter for various treatments. (e−h) Particle drag coefficient as a function of particle Reynolds number for different treatments. (a, e) Mineral deposition. Mass ratios of goethite to MPs were 1:50 (2GT), 1:20 (5GT), 1:10 (10GT), and 1:1 (100GT). (b, f) Chlorination. Concentrations used for the treatment were 2.0 g/L (2GL) and 4.0 g/L (4GL) (c, g) UV aging. UV aging for 3 days (UV-3 Day), 7 days (UV-7 Day), and 10 days (UV-10 Day). (d, h) OTS-coated (OTS) and functional grouping (−COOH, $-NH_2$); The Reynolds number and drag coefficients were calculated using eqs 1 and 2, respectively.

velocity increases (Figure 3a,b). The velocity was inversely correlated significantly to contact angle, as further confirmed by the correlation analysis (Figure 3c).

Our finding appears to be consistent with several prior studies. Al Harraq et al. found that increase in wettability (i.e., decreasing in contact angle) can cause MP having hydrophobic positive buoyancy to sink.[31] Pete et al. reported that biofilm formation can facilitate settlement of MPs likely due to increased wettability.[30] This suggests that wettability plays a crucial role in the settling of fine particles, with complex interplays of both molecular and particle scales. Therefore, when MPs undergo environmental aging—particularly due to UV irradiation and biofouling—the wettability of their surfaces can be altered, affecting their interaction with water and altering their settling velocities. The majority of negatively buoyant MPs (i.e., particles with densities exceeding that of water, such as those investigated in this study) demonstrate consistent settling behavior regardless of the weathering state. In contrast, neutrally buoyant particles exhibit weathering-dependent settling characteristics, as increased hydrophilicity reduces interfacial tension, thereby enhancing their propensity for gravitational settling.

As mentioned above, prior studies on MP settling predominantly emphasize morphological and physical parameters (e.g., particle geometry, size distribution, density gradients), and fewer examined the effects of surface properties on MP settling. As a result, the existing drag models show limited predictive accuracy for weathered MPs.[19,21] An improved model should capture the strong effects of surface chemistry alterations induced by environmental weathering on the hydrodynamic behavior of MPs in aquatic systems.

3.2. Evaluation and Expansion of the Modified Drag Model. *3.2.1. Comparison with the Existing Drag Model.* Unraveling the impact of surface properties on the settling kinetics of MPs remains a considerable challenge with limited studies quantifying how these properties influence MP settling. Understanding this effect is essential for clarifying the intricate interactions and behaviors of environmentally weathered MPs in aquatic systems. Environmental weathering modifies MP settling behavior by altering surface properties and adsorption capacity as these changes influence wettability and adjust the surface free energy of the particles.

The interfacial tension of particles represents the interactions between particles and liquids, offering insight into wetting, adsorption, and adhesion in the solid−liquid phases. To better define the relationship between the drag coefficient and the particle Reynolds number for MPs with varying wettability, MPs with a constant particle density were selected for nonlinear regression (Figures S3 and S6), incorporating the effects of particle interfacial tension. The remaining data set was then utilized to validate the proposed expression (eq 7).

$$\mathrm{Cd} = \frac{199.80}{\mathrm{Re}}\left(1 + 0.15\,\mathrm{Re}^{-3.74}\right)\mathrm{Eo}^{0.28} \tag{7}$$

The comparative analysis of drag coefficient predictions reveals critical limitations in existing models when applied to weathered MPs (Figure 4 and Table 3). While conventional models including those by Allen,[54] Clift and Gauvin,[53] Zhiyao et al.,[55] and Alcerreca et al.[57] demonstrate reasonable accuracy for pristine MPs (AE = 24.59−30.01%, Figure 4a−c,e), their performance degrades substantially (AE = 48.66%, Table 3) when predicting drag coefficients for MPs subjected to chlorination, UV aging, or surface coating. This deterioration stems from inadequate consideration of weathering-induced surface modifications such as wettability gradients, porosity development, and dynamic surface property alterations.[57]

While Wang et al.[29] developed a predictive model for wettability-dependent settling velocities using silica particles as the experimental substrate, its application to MPs reveals critical limitations. The model demonstrates restricted applicability (Re < 0.35), failing to accurately predict MP settling in transitional flow regimes (Re > 1, Figure 4g; AE = 50.71%). This divergence primarily stems from fundamental material differences: unlike natural sedimentary particles, MPs exhibit a lower density and inherent hydrophobicity. Environmental weathering induces surface oxidation and polymer degradation, modifying MP wettability and amplifying

https://doi.org/10.1021/acs.est.4c11053
Environ. Sci. Technol. XXXX, XXX, XXX−XXX

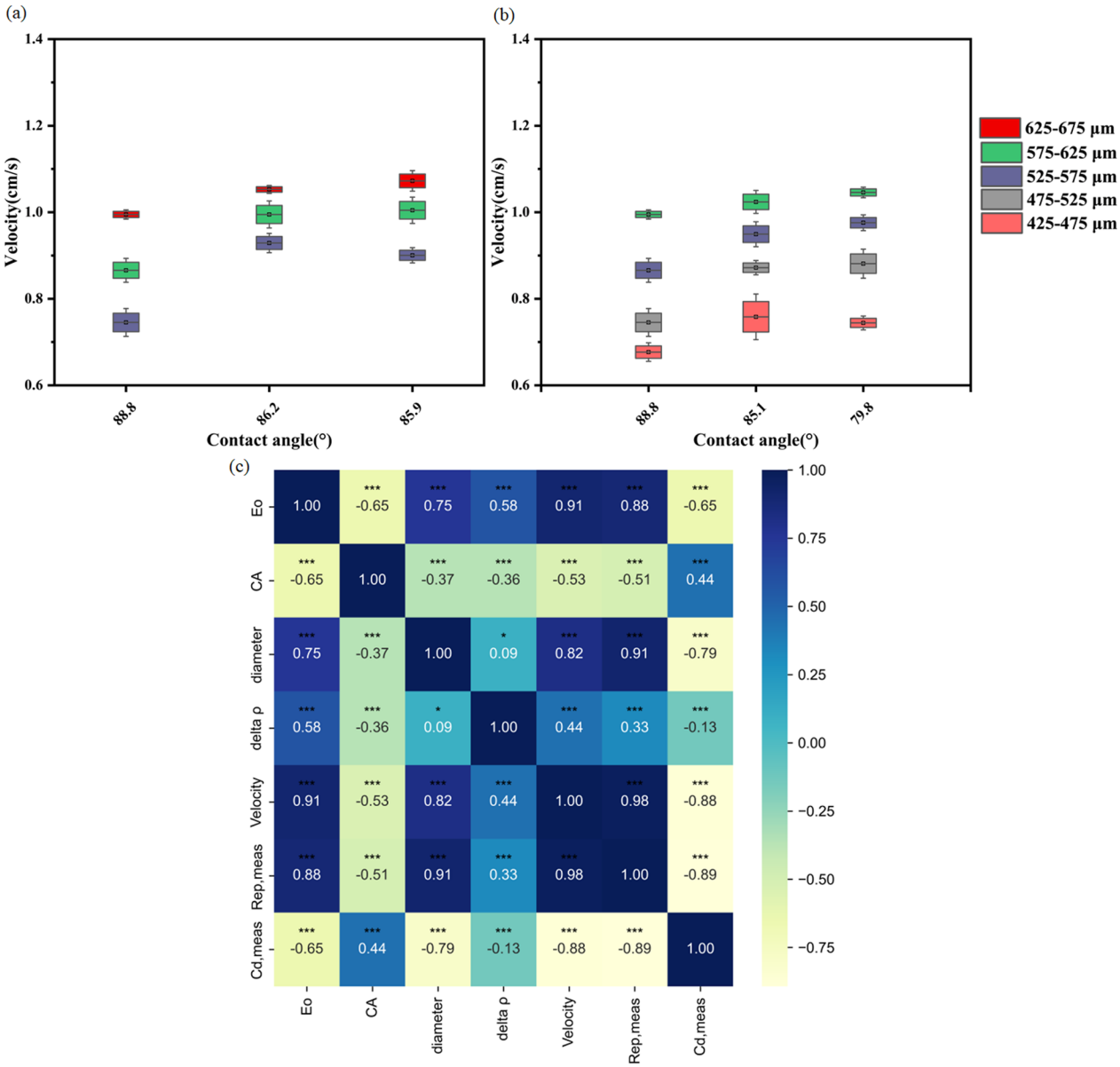

Figure 3. Relationship between contact angle and the settling velocity of MP in the small particle size range: (a) MP contact angle vs settling velocity after mineral deposition; (b) MP contact angle vs settling velocity after chlorination. (c) Spearman correlation analysis, CA: contact angle; *: $p < 0.05$; **: $0.001 \leq p < 0.01$; ***: $p < 0.001$

interfacial tension sensitivity—critical factors governing their hydrodynamic behavior. These physicochemical transformations introduce additional complexity to surface-mediated settling processes that conventional silica-based models cannot adequately capture.

Specialized MP models show mixed success (Figure 4, yellow background). Yu et al.[47] MP-shape formulation achieves moderate accuracy (AE = 33.42%, Figure 4k) but systematically underestimates drag coefficients for surface-modified particles. Shape-dependent models by Waldschläger and Schüttrumpf[60] and Wang et al.[61] exhibit particularly poor performance (AE = 85.81 and 76.23%, Figure 4i,j), likely due to their development for millimeter-scale particles. The model proposed by Zhang and Choi[62] exhibits systematic overprediction (AE = 52.39%, Figure 4l), while Khatmullina and Isachenko's formulation[59] demonstrates inverse underestimation trends (AE = 47.65%, Figure 4h).

Although methodologically innovative for biofilm-mediated surface modification, the roughness-dependent model proposed by Meng and Li[63] shows constrained predictive capability in wettability-governed MP systems (AE = 73.64%, Figure 4m). This discrepancy originates from distinct underlying mechanisms: although their approach considers biologically mediated roughness evolution via microbial activity, the present study quantifies physicochemical wettability transformations induced by environmental exposure. Roughness-based models struggle to accurately predict hydrophilicity-shifting MPs due to the absence of interfacial tension parametrization.

Our developed model (eq 7) works well for predicting spherically weathered MPs, reducing prediction errors by 21−74% (AE = 5.84−30.03 vs 7.86−90.44%; RMSE = 7.34−32.84 vs 10.49−90.48%, Table 3). This advancement stems from the explicit inclusion of wettability-dependent interfacial tension

https://doi.org/10.1021/acs.est.4c11053
Environ. Sci. Technol. XXXX, XXX, XXX−XXX

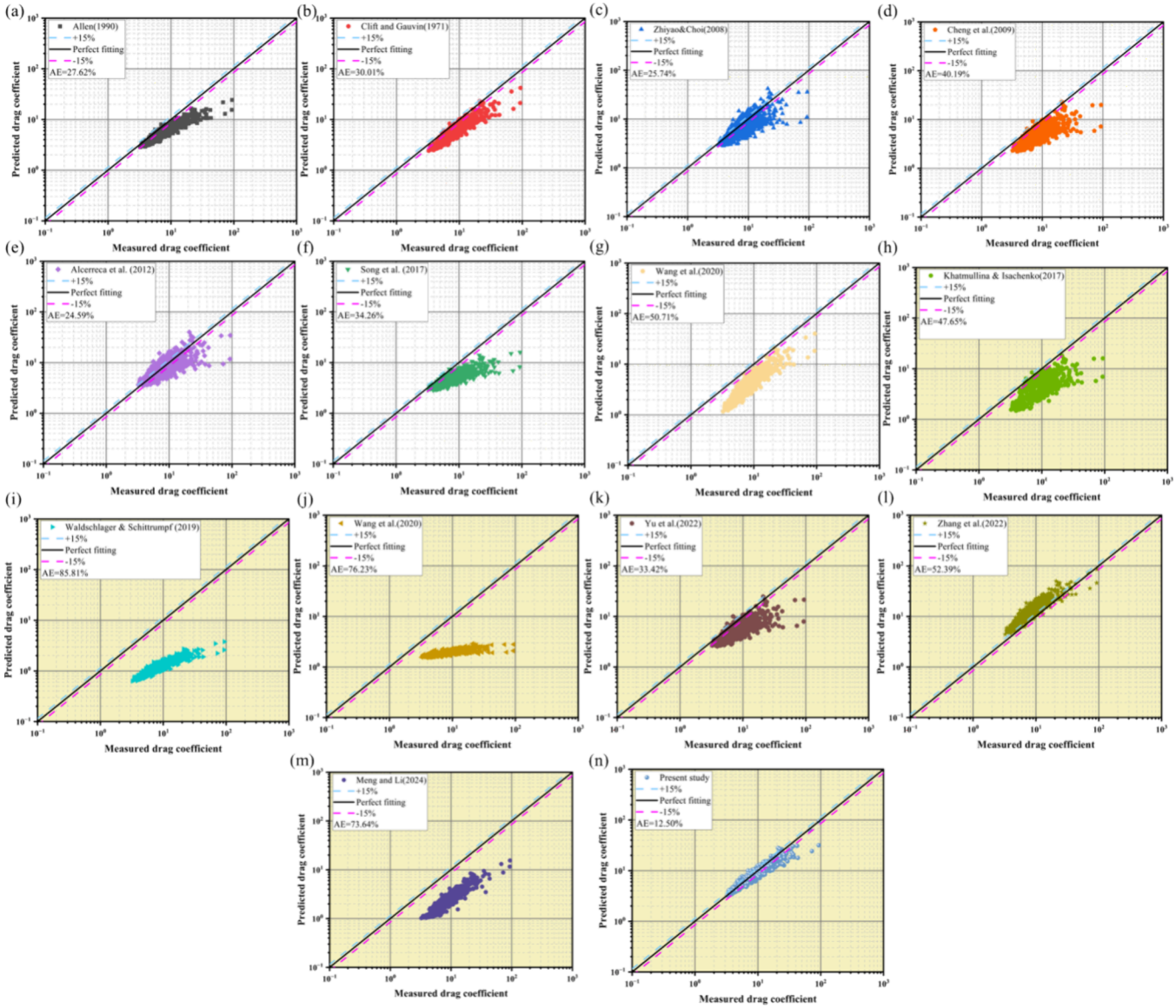

Figure 4. (a−n) Measured drag coefficient vs corresponding predictions by different models. Models derived specifically for MP are highlighted with a yellow background. (a) Allen,[54] (b) Clift and Gauvin,[53] (c) Zhiyao et al.,[55] (d) Cheng,[56] (e) Alcerreca et al.,[57] (f) Song et al.,[58] (g)Wang et al.,[29] (h) Khatmullina and Isachenko,[59] (i) Waldschläger and Schüttrumpf,[60] (j) Wang et al.,[61] (k) Yu et al.,[47] (l) Zhang and Choi,[62] (m) Meng and Li,[63] and (n) present study.

effects, enabling precise predictions of submillimeter MP settling across transitional flow regimes ($1 < Re < 20$).

3.2.2. Validation of the New Model on Different Data Sets. Figure 5a−c presents a comparative analysis of measured versus model-predicted drag coefficients for MPs across various data sets using the improved model (eq 7). The model demonstrated strong predictive accuracy for data set 2 and data set 5 (combined, AE = 15.97%, RMSE = 19.15%, Figure 5a). However, substantial discrepancies arose for data set 3 (AE = 48.96%, RMSE = 51.56%, Figure 5c), particularly in high-Reynolds conditions ($Re > 300$), where deviations approached 50%.

Similarly, the model exhibited limited applicability in the laminar regime (data set 4, fragmented MPs, $1 < Re$), with prediction errors spanning 6−7 orders of magnitude. Notably, Wang et al.'s model[29,34] achieved better accuracy in the laminar regime ($Re < 1$, AE = 31.58%) for data set 4 contact angle-varied MPs, reinforcing Eo′ as an effective wettability descriptor.

We infer that the impact of surface properties on resistance is dictated by flow regime: (1) the laminar regime ($Re < 1$), where wettability modulates boundary layer dynamics, (2) the transitional regime ($1 < Re < 300$), characterized by competing forces, and (3) the turbulent regime ($Re > 300$), where surface effects diminish. Further studies are needed to assess the model's reliability at higher Reynolds numbers.

For Yu et al.'s irregularly shaped MPs (data set 6),[47] the model revealed shape-dependent limitations (AE = 43.17%, RMSE = 47.28%, Figure 5b), though it maintained accuracy for spherical particles (AE = 7.51%, RMSE = 9.64%). The intentional spherical focus in eq 7 isolates surface wettability effects by minimizing shape-induced flow separation complexities, albeit at the cost of broader applicability to morphologically diverse MPs.

https://doi.org/10.1021/acs.est.4c11053
Environ. Sci. Technol. XXXX, XXX, XXX−XXX

Table 3. Average Relative Error and Root-Mean-Square Errors (AE and RMSE) of Different Model for MPs with Different Treatments

particle		metric	Allen[54]	Clift and Gauvin[53]	Zhiyao et al.[55]	Cheng[56]	Alcerreca et al.[57]	Song et al.[58]	Khatmullina and Isachenko[59]	Waldschläger and Schüttrumpf[60]	Wang et al.[29]	Wang et al.[61]	Zhang and Choi[62]	Yu et al.[47]	Meng and Li[63]	present study
origin		AE (%)	26.30	28.25	13.38	39.32	7.86	33.04	40.91	85.73	48.77	78.13	56.93	32.22	75.74	5.84
		RMSE (%)	27.38	28.59	15.76	39.89	10.49	33.87	41.49	85.76	49.01	78.29	57.78	33.16	75.77	7.34
OTS		AE (%)	48.66	46.30	45.16	62.63	40.13	58.45	63.30	90.44	60.07	87.47	27.61	58.08	71.53	30.03
		RMSE (%)	50.42	47.83	48.86	63.66	44.73	60.20	64.56	90.48	60.67	87.60	32.96	59.86	71.80	32.84
mineral deposition		AE (%)	24.41	25.00	24.23	34.47	26.43	28.31	39.90	85.44	45.05	77.22	64.84	27.73	71.17	11.77
		RMSE (%)	28.4	28.74	31.03	38.77	31.53	33.95	44.21	85.49	47.06	77.49	72.70	33.45	71.36	14.49
chlorination		AE (%)	16.27	20.01	12.82	27.29	20.94	20.19	28.12	83.61	43.19	74.01	75.67	19.22	74.32	9.44
		RMSE (%)	18.95	21.63	17.78	29.46	24.76	23.45	30.26	83.64	43.66	74.16	77.41	22.69	74.38	11.66
UV-aging		AE (%)	41.49	41.79	38.23	56.51	31.12	52.02	68.48	88.83	56.78	82.02	28.37	51.38	77.27	13.92
		RMSE (%)	42.45	42.33	40.07	57.19	33.83	52.93	68.80	88.85	56.95	82.16	31.08	52.34	77.30	15.49
functional grouping	COOH	AE (%)	17.78	27.50	18.69	33.09	15.31	26.49	53.42	82.69	56.92	62.90	47.22	24.88	74.54	9.92
		RMSE (%)	20.44	29.27	22.48	35.58	21.07	29.44	54.27	82.72	57.48	63.20	52.27	27.99	74.62	13.48
	NH_2	AE (%)	21.98	32.74	23.36	39.09	15.88	32.15	58.25	83.29	63.06	62.66	32.47	30.27	74.71	9.69
		RMSE (%)	24.51	34.06	26.96	40.95	19.49	34.89	58.89	83.33	63.33	63.02	37.12	33.25	74.81	11.85

https://doi.org/10.1021/acs.est.4c11053
Environ. Sci. Technol. XXXX, XXX, XXX−XXX

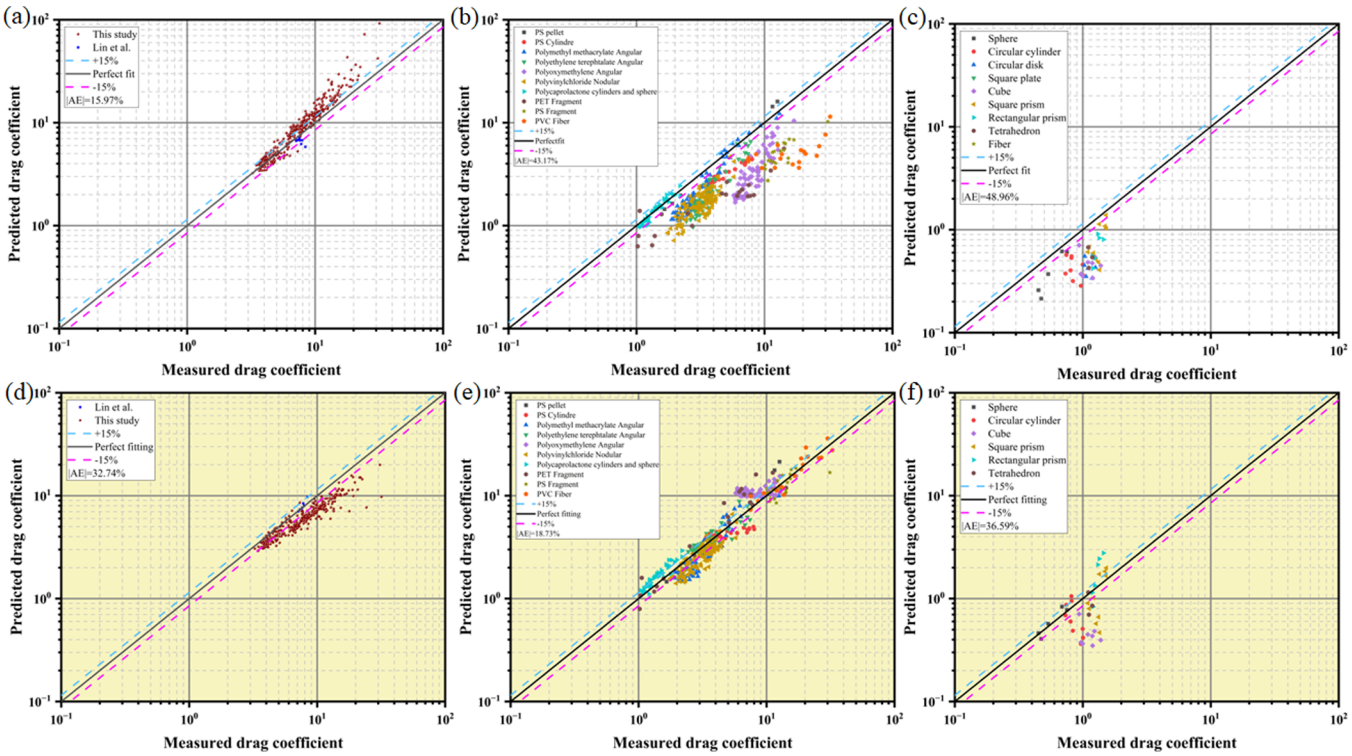

Figure 5. Prediction of the improved model (eq 7 with white background and eq 8 with yellow background) for different MP settling velocity data sets. (a, d) Data set 2 and data set 5 (Lin et al.'s data set with validation set in this study). Spherical MPs have different contact angles and the particles are in the transition flow regime ($1 < Re < 23$). (b, e) Data set 6 (Yu et al.'s data set). MPs with fragment, nodular, sphere, and particles are in transition regime ($2 < Re < 285$). (c, f) Data set 3 (Goral et al.'s data set). MPs with rectangular prism, square prism, cube, circular cylinder, (except square plate and circular disk), and the particles are in the transition regime ($73 < Re < 1134$).

3.2.3. Expansion for Different Shapes of Plastics. To improve the generality of the model, the shape factor was integrated in the model, which was further validated using reported data. The refined model (eq 8) demonstrated validation efficacy across multiple data sets: data set 6 (AE = 18.73%, RMSE = 23.70%, Figure 5e). Data set 5 (AE = 13.31%, RMSE = 18.75%) and data set 2 (AE = 33.15%, RMSE = 36.90%) combined (AE = 32.74%, RMSE = 36.63%, Figure 5d). Notably, the contact angle inputs were derived from secondary literature sources rather than direct experimental measurements, introducing inherent uncertainties from (i) polymer additive variations and (ii) surface−adsorbate heterogeneity. These material-dependent variations, compounded by potential changes in surface properties induced by compression during sample preparation, represent the primary sources of error in the current model (eq 8).

$$Cd = \frac{47.145 Eo^{0.342} Cd_s}{(d_*^{7.6938} \Phi^{d_*^{-2.2510}} CSF^{d_*^{0.6479}})^{0.128}} \quad (8)$$

$$Cd_s = \frac{432}{d_*^3}(1 + 0.022 d_*^3)^{0.54} + 0.47[1 - \exp(-0.15 d_*^{0.45})] \quad (9)$$

where $d_* = \left[\frac{(\rho_s - \rho_1)g}{\rho_1 \nu^2}\right]^{1/3} d_n$ and $CSF = \frac{c}{(ab)^{0.5}}$ where a, b, and c are the lengths of the longest, intermediate, and shortest sides of a particle, respectively. The range of core shape factor (CSF) is 0−1, where 0 is for a disk and 1 is for a cube or a sphere. Sphericity ($\Phi = \frac{A_{sph}}{A_s}$) was used to describe their difference compared to perfect spheres ($\Phi = 1$), where A_s is the surface area of the real particle and $A_{sph} = 4\pi(d_{n/2})^2$ is the surface area of the volume-equivalent sphere.

For data set 3, while the AE reached 149.86%, the model maintained good accuracy (AE = 36.59%, Figure 5f when excluding plate-like MPs. This is due to the settling orientation of disks along the trajectory impacts the Cd−Re relationship.[67] In addition, Data set 3 had a high Re = 73 to 1135. At higher Reynolds numbers, it is possible that the effect of wettability is relatively weak. This is likely due to the settling orientation of disk-shaped particles, which influences their interaction with the surrounding fluid and, in turn, modifies the drag forces. We infer that the unsteady sinking motion of disks or sheets generates turbulent disturbances in the fluid, potentially masking the effects of the surface wettability. This may explain the model's inaccuracies at high Reynolds numbers. MPs occur in a wide range of shapes—including cylinders, discs, granules, fibers, fragments, and films—with different core shape factors (CSF, distinguish MP fragments and fibers) and sphericity (Φ, distinction MP films and nonfilm MPs). It is likely that the influence of wettability diminishes as particle shapes deviate further from spheres. The specific impact of wettability on the settling behavior of sheet-like or disk-like MPs remains an area for further investigation.

Our model demonstrates complementary strengths: eq 7 excels for spherical MPs ($1 < Re < 20$), while eq 8 extends applicability to morphologically complex MPs ($1 < Re < 200$) through incorporation of CSF and Φ. However, it is important to note that the new model (eqs 7 and 8) does not account for the potential influence of environmental factors. For instance,

https://doi.org/10.1021/acs.est.4c11053
Environ. Sci. Technol. XXXX, XXX, XXX−XXX

seasonal variations can alter the physical properties of water—such as temperature, density, and viscosity—which may affect the model's accuracy. Furthermore, the surface wettability of MPs evolves dynamically during long-term natural weathering, resulting in a nonlinear superposition of drag coefficients. The applicability of the model in complex, real-world environments remains to be further investigated.

3.3. Environmental Implications. This study demonstrated that the terminal settling velocity of submillimeter MPs is affected by their wettability, which could significantly influence their environmental behavior and fate. The inherent wettability and hydrophobicity of pristine MPs gradually transform through weathering processes such as photo-oxidation, biofilm formation, and contaminant sorption. The drag model we proposed and evaluated in this study is derived primarily based on our current findings for variously weathered MPs. Specifically, it counts for changes in wettability due to weathering processes. Our parametric analysis indicates that decreased contact angle or enhanced hydrophilicity can accelerate settling velocity, contingent on particle size and fluid flow conditions. The proposed Eo′-based drag model (eqs 7 and 8) effectively quantifies this surface-dependent transport modification.

Compared to conventional models that often overlook wettability effects, our newly developed Eo′-based drag model provides an accurate prediction of MP settling velocity in aquatic systems. By explicitly incorporating wettability-driven variations in drag force, this model accounts for the progressive surface modifications that MPs undergo in natural environments. Our results show that for hydrophilic MPs, the predicted settling velocities align more closely with experimental measurements, reducing discrepancies observed in previous models.

Despite the model improvements made in this study for predicting MP drag coefficients, challenges persist. The refined model (eqs 7 and 8) does not demonstrate significantly improved accuracy in estimating drag coefficients within the laminar and turbulent flow regimes. This suggests that the model may have limitations in environments with stronger hydrodynamic conditions, such as estuaries and areas with current disturbances. Additionally, the mixing of freshwater and seawater in estuary systems creates complex flow hierarchies that the model does not currently address. Moreover, the study only examined the effects of iron oxide mineral deposition on MP surfaces, whereas in turbid water MPs may interact with a variety of suspended particles, each potentially influencing MP wettability to different extents. As a result, the applicability of the refined model under real environmental conditions remains uncertain. To enhance model applicability, future research should focus on simultaneous evaluation of the combined contact angle-settling velocity, shape factor relationship, and environmental conditions under controlled aging conditions and the extent to which surface properties respond to the complexity of the environment. This integrated approach would facilitate linking surface weathering effects to turbulent flow interactions.

■ ASSOCIATED CONTENT

Supporting Information

The Supporting Information is available free of charge at https://pubs.acs.org/doi/10.1021/acs.est.4c11053.

Data sets for this experiment, Goral et. al., Dittmar et al., Lin et., and Yu et al.; data for fitting; data for validation (XLSX)

Supplementary sections, figures, and references (PDF)

■ AUTHOR INFORMATION

Corresponding Author

Chen Yang − *College of Environment and Energy, South China University of Technology, Guangzhou 510006, China; The Key Lab of Pollution Control and Ecosystem Restoration in Industry Clusters, Ministry of Education, Guangzhou 510006, China;* orcid.org/0000-0001-7205-1016; Email: cyanggz@scut.edu.cn

Authors

Yi Liang − *College of Environment and Energy, South China University of Technology, Guangzhou 510006, China*

Jingyi Gu − *College of Environment and Energy, South China University of Technology, Guangzhou 510006, China*

Ketong Chen − *College of Environment and Energy, South China University of Technology, Guangzhou 510006, China*

Hong Zhou − *College of Environment and Energy, South China University of Technology, Guangzhou 510006, China*

Jiamin Peng − *College of Environment and Energy, South China University of Technology, Guangzhou 510006, China*

Tingting Cai − *College of Environment and Energy, South China University of Technology, Guangzhou 510006, China*

Pei Na − *College of Environment and Energy, South China University of Technology, Guangzhou 510006, China*

Chenlu Guo − *College of Environment and Energy, South China University of Technology, Guangzhou 510006, China*

Weilin Huang − *Department of Environmental Sciences, Rutgers, The State University of New Jersey, New Brunswick, New Jersey 08901, United States*

Zhi Dang − *College of Environment and Energy, South China University of Technology, Guangzhou 510006, China; The Key Lab of Pollution Control and Ecosystem Restoration in Industry Clusters, Ministry of Education, Guangzhou 510006, China*

Complete contact information is available at: https://pubs.acs.org/10.1021/acs.est.4c11053

Notes

The authors declare no competing financial interest.

■ ACKNOWLEDGMENTS

This study was supported by the National Natural Science Foundation of China (no. 42077337) and Science and Technology Planning Project of Guangdong Province (2024B1212050009). The surface roughness test was conducted at Shanghai Sensofar Tech Co., Ltd (China). We would also like to express our sincere appreciation to the four anonymous reviewers and the editor for their insightful comments and constructive feedback, which have significantly contributed to enhancing the quality of this study.

■ REFERENCES

(1) Kelly, A.; Lannuzel, D.; Rodemann, T.; Meiners, K. M.; Auman, H. J. Microplastic Contamination in East Antarctic Sea Ice. *Mar. Pollut. Bull.* **2020**, *154*, No. 111130.

(2) Hoang, V.-H.; Nguyen, M.-K.; Hoang, T.-D.; Ha, M. C.; Huyen, N. T. T.; Bui, V. K. H.; Pham, M.-T.; Nguyen, C.-M.; Chang, S. W.; Nguyen, D. D. Sources, Environmental Fate, and Impacts of

Microplastic Contamination in Agricultural Soils: A Comprehensive Review. *Science of The Total Environment* **2024**, *950*, No. 175276.
(3) Sun, J.; Peng, Z.; Zhu, Z.-R.; Fu, W.; Dai, X.; Ni, B.-J. The Atmospheric Microplastics Deposition Contributes to Microplastic Pollution in Urban Waters. *Water Res.* **2022**, *225*, No. 119116.
(4) Silva-Cavalcanti, J. S.; Silva, J. D. B.; de França, E. J.; de Araújo, M. C. B.; Gusmão, F. Microplastics Ingestion by a Common Tropical Freshwater Fishing Resource. *Environ. Pollut.* **2017**, *221*, 218−226.
(5) Vroom, R. J. E.; Koelmans, A. A.; Besseling, E.; Halsband, C. Aging of Microplastics Promotes Their Ingestion by Marine Zooplankton. *Environ. Pollut.* **2017**, *231*, 987−996.
(6) Chubarenko, I.; Bagaev, A.; Zobkov, M.; Esiukova, E. On Some Physical and Dynamical Properties of Microplastic Particles in Marine Environment. *Mar. Pollut. Bull.* **2016**, *108* (1), 105−112.
(7) Cowger, W.; Gray, A. B.; Guilinger, J. J.; Fong, B.; Waldschläger, K. Concentration Depth Profiles of Microplastic Particles in River Flow and Implications for Surface Sampling. *Environ. Sci. Technol.* **2021**, *55* (9), 6032−6041.
(8) Sun, Y.; Cao, L.; Wang, Y.; Chen, W.; Li, Y.; Zhao, X. Sources and Distribution of Microplastics in the East China Sea under a Three-Dimensional Numerical Modelling. *Environ. Pollut.* **2022**, *311*, No. 119910.
(9) Dai, J.; Liu, P.; Wang, C.; Li, H.; Qiang, H.; Yang, Z.; Guo, X.; Gao, S. Which Factors Mainly Drive the Photoaging of Microplastics in Freshwater? *Science of The Total Environment* **2023**, *858*, No. 159845.
(10) Laursen, S. N.; Fruergaard, M.; Dodhia, M. S.; Posth, N. R.; Rasmussen, M. B.; Larsen, M. N.; Shilla, D.; Shilla, D.; Kilawe, J. J.; Kizenga, H. J.; Andersen, T. J. Settling of Buoyant Microplastic in Estuaries: The Importance of Flocculation. *Science of The Total Environment* **2023**, *886*, No. 163976.
(11) Liro, M.; Zielonka, A.; van Emmerik, T. H. M. Macroplastic Fragmentation in Rivers. *Environ. Int.* **2023**, *180*, No. 108186.
(12) Nguyen, T. H.; Tang, F. H. M.; Maggi, F. Sinking of Microbial-Associated Microplastics in Natural Waters. *PLoS One* **2020**, *15* (2), No. e0228209.
(13) Stead, J. L.; Bond, T. The Impact of Riverine Particles on the Vertical Velocities of Large Microplastics. *Science of The Total Environment* **2023**, *896*, No. 165339.
(14) Leiser, R.; Wu, G.-M.; Neu, T. R.; Wendt-Potthoff, K. Biofouling, Metal Sorption and Aggregation Are Related to Sinking of Microplastics in a Stratified Reservoir. *Water Res.* **2020**, *176*, No. 115748.
(15) Wang, Y.; Chen, X.; Wang, F.; Cheng, N. Influence of Typical Clay Minerals on Aggregation and Settling of Pristine and Aged Polyethylene Microplastics. *Environ. Pollut.* **2023**, *316*, No. 120649.
(16) Yang, X.; Huang, G.; Chen, Z.; Feng, Q.; An, C.; Lyu, L.; Bi, H.; Zhou, S. Spotlight on the Vertical Migration of Aged Microplastics in Coastal Waters. *Journal of Hazardous Materials* **2024**, *469*, No. 134040.
(17) Kaiser, D.; Kowalski, N.; Waniek, J. J. Effects of Biofouling on the Sinking Behavior of Microplastics. *Environ. Res. Lett.* **2017**, *12* (12), 124003.
(18) Kowalski, N.; Reichardt, A. M.; Waniek, J. J. Sinking Rates of Microplastics and Potential Implications of Their Alteration by Physical, Biological, and Chemical Factors. *Mar. Pollut. Bull.* **2016**, *109* (1), 310−319.
(19) Brooks, J. M.; Boyer, J. J.; Haberstroh, C. J.; Arias, M. E. Settling Velocities of Environmentally Weathered Plastic Fibers from the Mekong River in Southeast Asia. *ACS EST Water* **2024**, *4* (4), 1556−1563.
(20) Dittmar, S.; Ruhl, A. S.; Altmann, K.; Jekel, M. Settling Velocities of Small Microplastic Fragments and Fibers. *Environ. Sci. Technol.* **2024**, *58* (14), 6359−6369.
(21) Kaiser, D.; Estelmann, A.; Kowalski, N.; Glockzin, M.; Waniek, J. J. Sinking Velocity of Sub-Millimeter Microplastic. *Mar. Pollut. Bull.* **2019**, *139*, 214−220.
(22) Waldschläger, K.; Born, M.; Cowger, W.; Gray, A.; Schüttrumpf, H. Settling and Rising Velocities of Environmentally Weathered Micro- and Macroplastic Particles. *Environmental Research* **2020**, *191*, No. 110192.
(23) Chen, X.; Xiong, X.; Jiang, X.; Shi, H.; Wu, C. Sinking of Floating Plastic Debris Caused by Biofilm Development in a Freshwater Lake. *Chemosphere* **2019**, *222*, 856−864.
(24) Gopalakrishnan, K.; Kashian, D. R. Extracellular Polymeric Substances in Green Alga Facilitate Microplastic Deposition. *Chemosphere* **2022**, *286*, No. 131814.
(25) Sooriyakumar, P.; Bolan, N.; Kumar, M.; Singh, L.; Yu, Y.; Li, Y.; Weralupitiya, C.; Vithanage, M.; Ramanayaka, S.; Sarkar, B.; Wang, F.; Gleeson, D. B.; Zhang, D.; Kirkham, M. B.; Rinklebe, J.; M Siddique, K. H. Biofilm Formation and Its Implications on the Properties and Fate of Microplastics in Aquatic Environments: A Review. *Journal of Hazardous Materials Advances* **2022**, *6*, No. 100077.
(26) Beratlis, N.; Balaras, E.; Squires, K. The Role of Surface Texturing on the Physics of Boundary Layer Separation over a Bump. *International Journal of Heat and Fluid Flow* **2018**, *73*, 223−235.
(27) Choi, J.; Jeon, W.-P.; Choi, H. Mechanism of Drag Reduction by Dimples on a Sphere. *Phys. Fluids* **2006**, *18* (4), No. 041702.
(28) Villa, S.; Boniello, G.; Stocco, A.; Nobili, M. Motion of Micro- and Nano- Particles Interacting with a Fluid Interface. *Adv. Colloid Interface Sci.* **2020**, *284*, No. 102262.
(29) Wang, L.; Zheng, K.; Ding, Z.; Yan, X.; Zhang, H.; Cao, Y.; Guo, C. Drag Coefficient and Settling Velocity of Fine Particles with Varying Surface Wettability. *Powder Technol.* **2020**, *372*, 8−14.
(30) Pete, A. J.; Brahana, P. J.; Bello, M.; Benton, M. G.; Bharti, B. Biofilm Formation Influences the Wettability and Settling of Microplastics. *Environ. Sci. Technol. Lett.* **2023**, *10* (2), 159−164.
(31) Al Harraq, A.; Brahana, P. J.; Arcemont, O.; Zhang, D.; Valsaraj, K. T.; Bharti, B. Effects of Weathering on Microplastic Dispersibility and Pollutant Uptake Capacity. *ACS Environ. Au* **2022**, *2* (6), 549−555.
(32) Jiang, X.; Wang, T.; Jiang, M.; Xu, M.; Yu, Y.; Guo, B.; Chen, D.; Hu, S.; Jiang, J.; Zhang, Y.; Zhu, B. Assessment of Plastic Stocks and Flows in China: 1978−2017. *Resources, Conservation and Recycling* **2020**, *161*, No. 104969.
(33) Belesov, A. V.; Rezviy, T. V.; Pokryshkin, S. A.; Lakhmanov, D. E.; Chukhchin, D. G.; Kozhevnikov, A. Y. Impact of Coastal Sediments of the Northern Dvina River on Microplastics Inputs to the White and Barents Seas. *Journal of Marine Science and Engineering* **2022**, *10* (10), 1485.
(34) Yuan, Z.; Nag, R.; Cummins, E. Ranking of Potential Hazards from Microplastics Polymers in the Marine Environment. *Journal of Hazardous Materials* **2022**, *429*, No. 128399.
(35) Ma, J.; Jing, Y.; Gao, L.; Chen, J.; Wang, Z.; Weng, L.; Li, H.; Chen, Y.; Li, Y. Hetero-Aggregation of Goethite and Ferrihydrite Nanoparticles Controlled by Goethite Nanoparticles with Elongated Morphology. *Science of The Total Environment* **2020**, *748*, No. 141536.
(36) Wang, J.; Wang, H.; Yue, D. Insights into Mechanism of Hypochlorite-Induced Functionalization of Polymers toward Separating BFR-Containing Components from Microplastics. *ACS Appl. Mater. Interfaces* **2020**, *12* (32), 36755−36767.
(37) Zang, D.; Liu, F.; Zhang, M.; Niu, X.; Gao, Z.; Wang, C. Superhydrophobic Coating on Fiberglass Cloth for Selective Removal of Oil from Water. *Chemical Engineering Journal* **2015**, *262*, 210−216.
(38) Zhang, L.; Zhou, A. G.; Sun, B. R.; Chen, K. S.; Yu, H.-Z. Functional and Versatile Superhydrophobic Coatings via Stoichiometric Silanization. *Nat. Commun.* **2021**, *12* (1), 982.
(39) Dietrich, W. E. Settling Velocity of Natural Particles. *Water Resour. Res.* **1982**, *18* (6), 1615−1626.
(40) Van Melkebeke, M.; Janssen, C.; De Meester, S. Characteristics and Sinking Behavior of Typical Microplastics Including the Potential Effect of Biofouling: Implications for Remediation. *Environ. Sci. Technol.* **2020**, *54* (14), 8668−8680.
(41) Lin, J.; Wu, X.; Liu, Y.; Fu, J.; Chen, Y.; Ou, H. Sinking Behavior of Polystyrene Microplastics after Disinfection. *Chemical Engineering Journal* **2022**, *427*, No. 130908.
(42) Ji, B.; Song, Q.; Yao, Q. Limit for Small Spheres To Float by Dynamic Analysis. *Langmuir* **2018**, *34* (34), 10163−10168.

https://doi.org/10.1021/acs.est.4c11053
Environ. Sci. Technol. XXXX, XXX, XXX−XXX

(43) Hager, W. H. Wilfrid Noel Bond and the Bond Number. *Journal of Hydraulic Research* **2012**, *50* (1), 3−9.
(44) Zhu, D.; Dai, P.; Luo, X.; Zhang, Y. Novel Characterization of Wetting Properties and the Calculation of Liquid-Solid Interface Tension. *Sci. Technol. Eng.* **2007**, *7* (2007), 3067−3072.
(45) Tang, Q.; Qin, X.; Dong, H.; Zhang, X.; Wang, X.; Wang, K. Novel Drag Coefficient Models of Ionic Liquid − Spherical Particle System. *Chem. Eng. Sci.* **2019**, *204*, 177−185.
(46) Goral, K. D.; Guler, H. G.; Larsen, B. E.; Carstensen, S.; Christensen, E. D.; Kerpen, N. B.; Schlurmann, T.; Fuhrman, D. R. Settling Velocity of Microplastic Particles Having Regular and Irregular Shapes. *Environmental Research* **2023**, *228*, No. 115783.
(47) Yu, Z.; Yang, G.; Zhang, W. A New Model for the Terminal Settling Velocity of Microplastics. *Mar. Pollut. Bull.* **2022**, *176*, No. 113449.
(48) Chodkowski, M.; Terpiłowski, K.; Románszki, L.; Klébert, S.; Mohai, M.; Károly, Z. Effect of Non-Thermal Sulfur Hexafluoride Cold Plasma Modification on Surface Properties of Polyoxymethylene. *ChemPhysChem* **2024**, *25* (10), No. e202300709.
(49) Zdziennicka, A.; Szymczyk, K.; Krawczyk, J.; Jańczuk, B. Some Remarks on the Solid Surface Tension Determination from Contact Angle Measurements. *Appl. Surf. Sci.* **2017**, *405*, 88−101.
(50) Kim, K.-R.; Park, J.-W.; Cho, E.; Jang, Y.-A.; Eom, G. T.; Oh, Y.-R. Isolation of a Halotolerant Poly(ε-Caprolactone)-Depolymerizing Strain of Bacillus Gibsonii from Seaside Soil. *Biotechnol Bioproc E* **2024**, *29* (5), 815−824.
(51) Pita, F.; Castilho, A. Separation of Plastics by Froth Flotation. The Role of Size, Shape and Density of the Particles. *Waste Management* **2017**, *60*, 91−99.
(52) Zheng, M.; Wu, P.; Li, L.; Yu, F.; Ma, J. Adsorption/Desorption Behavior of Ciprofloxacin on Aged Biodegradable Plastic PLA under Different Exposure Conditions. *Journal of Environmental Chemical Engineering* **2023**, *11* (1), No. 109256.
(53) Clift, R.; Gauvin, W. H. Motion of Entrained Particles in Gas Streams. *Canadian Journal of Chemical Engineering* **1971**, *49* (4), 439−448.
(54) Allen, H. S. XXXI. The Motion of a Sphere in a Viscous Fluid. *London, Edinburgh, and Dublin Philosophical Magazine and Journal of Science* **1900**, *50* (304), 323−338.
(55) Zhiyao, S.; Tingting, W.; Fumin, X.; Ruijie, L. A Simple Formula for Predicting Settling Velocity of Sediment Particles. *Water Science and Engineering* **2008**, *1* (1), 37−43.
(56) Cheng, N.-S. Comparison of Formulas for Drag Coefficient and Settling Velocity of Spherical Particles. *Powder Technol.* **2009**, *189* (3), 395−398.
(57) Alcerreca, J. C.; Silva, R.; Mendoza, E. Simple Settling Velocity Formula for Calcareous Sand. *Journal of Hydraulic Research* **2013**, *51* (2), 215−219.
(58) Song, X.; Xu, Z.; Li, G.; Pang, Z.; Zhu, Z. A New Model for Predicting Drag Coefficient and Settling Velocity of Spherical and Non-Spherical Particle in Newtonian Fluid. *Powder Technol.* **2017**, *321*, 242−250.
(59) Khatmullina, L.; Isachenko, I. Settling Velocity of Microplastic Particles of Regular Shapes. *Mar. Pollut. Bull.* **2017**, *114* (2), 871−880.
(60) Waldschläger, K.; Schüttrumpf, H. Effects of Particle Properties on the Settling and Rise Velocities of Microplastics in Freshwater under Laboratory Conditions. *Environ. Sci. Technol.* **2019**, *53* (4), 1958−1966.
(61) Wang, Z.; Dou, M.; Ren, P.; Sun, B.; Jia, R.; Zhou, Y. Settling Velocity of Irregularly Shaped Microplastics under Steady and Dynamic Flow Conditions. *Environ. Sci. Pollut Res.* **2021**, *28* (44), 62116−62132.
(62) Zhang, J.; Choi, C. E. Improved Settling Velocity for Microplastic Fibers: A New Shape-Dependent Drag Model. *Environ. Sci. Technol.* **2022**, *56* (2), 962−973.
(63) Meng, D.; Li, Y. Assessing the Settling Velocity of Biofilm-Encrusted Microplastics: Accounting for Biofilms as an Equivalent to Surface Roughness. *Environ. Sci. Technol.* **2024**, *58* (2), 1329−1337.
(64) Alimi, O. S.; Claveau-Mallet, D.; Lapointe, M.; Biu, T.; Liu, L.; Hernandez, L. M.; Bayen, S.; Tufenkji, N. Effects of Weathering on the Properties and Fate of Secondary Microplastics from a Polystyrene Single-Use Cup. *Journal of Hazardous Materials* **2023**, *459*, No. 131855.
(65) Anderson, J. D., Jr. Ludwig Prandtl's Boundary Layer. *Phys. Today* **2005**, *58* (12), 42−48.
(66) Brahana, P.; Zhang, M.; Nakouzi, E.; Bharti, B. Weathering Influences the Ice Nucleation Activity of Microplastics. *Nat. Commun.* **2024**, *15* (1), 9579.
(67) Yang, G.; Yu, Z.; Baki, A. B. M.; Yao, W.; Ross, M.; Chi, W.; Zhang, W. Settling Behaviors of Microplastic Disks in Water. *Mar. Pollut. Bull.* **2023**, *188*, No. 114657.

https://doi.org/10.1021/acs.est.4c11053
Environ. Sci. Technol. XXXX, XXX, XXX−XXX